Atomic barium and cesium alignment-to-orientation conversion in external electric and magnetic fields

Robert C. Hilborn, Larry R. Hunter, Kent Johnson,* Stephen K. Peck, Alison Spencer,† and John Watson‡
Department of Physics, Amherst College, Amherst, Massachusetts 01002
(Received 7 March 1994)

We present an alternative method for changing atomic alignment to orientation through interactions with orthogonal static electric and magnetic fields. Experimental results demonstrating this effect in the $5d6p\ ^1P$ state of atomic barium and the $F=4$ hyperfine level of the ground state of atomic cesium are presented. The theory of this effect for a $j=0$ to $j=1$ electric dipole transition is discussed in detail. The tensor polarizability of the $5d6p\ ^1P$ state of Ba is determined to be 1.31(15) MHz/(kV/cm)^2, in good agreement with the results of van Leeuwen and Hogervorst [Z. Phys. A **310**, 37 (1983)].

PACS number(s): 32.80.Bx, 32.60.+i, 35.10.Di

I. INTRODUCTION

A. Context

There is considerable interest in methods of producing controlled atomic and molecular alignment and orientation and understanding various mechanisms that produce or destroy alignment and orientation. Most interatomic and intermolecular interactions depend strongly on the relative orientation of the interacting partners. In addition, many atomic physics experiments use the appearance of atomic orientation or changes in the direction of atomic orientation as a signal for parity-violating or time-reversal-invariance-violating interactions [1–3].

An atomic or molecular system is said to be oriented if states labeled by the magnetic quantum numbers m and $-m$ have different populations. On the other hand, if a state's population depends on the different absolute values $|m|$, the system is said to be aligned. In more formal terms we may define the orientation and alignment of a system in terms of expectation values of its angular momentum operators. Specifically, for a state of definite angular momentum j, the degree of orientation along the z axis is given [4] by

$$O_0=\frac{\langle \hat{J}_z \rangle}{j(j+1)} . \tag{1}$$

(Throughout this paper we shall use dimensionless angular momentum operators.) The degree of alignment is described by three parameters:

$$A_0=\frac{\langle 3\hat{J}_z^2-\hat{J}^2 \rangle}{j(j+1)} ,$$
$$A_{2+}=\frac{\langle \hat{J}_x^2-\hat{J}_y^2 \rangle}{j(j+1)} , \tag{2}$$
$$A_{1+}=\frac{\langle J_xJ_z+J_zJ_x \rangle}{j(j+1)} .$$

As is well known, and as we shall discuss explicitly below, the electronic orientation of a $j=1$ atomic state may be monitored directly by detecting the difference in intensities of left- and right-circularly polarized light emitted from that state. The connection between the observed light polarization and the system's orientation and alignment has been discussed in detail for atoms [4] and molecules [5]. For states with higher j values, we need to measure all of the Stokes parameters of the emitted light to determine the orientation. The relationship between the measured Stokes parameters and the degree of orientation and alignment is readily available [6]. Conversely, the observation of a net circular polarization in the light emission from some atomic source, say in a stellar atmosphere [7], implies a net orientation of the emitting atoms.

Alignment is produced by almost any anisotropic interaction. Any collisional or radiative excitation, for example, whether polarized or unpolarized, will produce an aligned system if the excitation is anisotropic [8]. We are interested in mechanisms that can cause an initially aligned atomic or molecular system to evolve into an oriented system. We call this process alignment-to-orientation conversion (AOC).

B. Symmetry considerations

Since the orientation of a system relative to some z axis is proportional to the average (expectation) value of the z component of the angular momentum $\langle J_z \rangle$, the orientation has the symmetry character of an axial vector and is even under P (spatial inversion) but odd under T (time re-

*Present address: Department of Physics, Harvard University, Cambridge, MA 02138.
†Present address: Oxford University, Oxford, England.
‡Present address: Department of Physics, Northwestern University, Evanston, IL 60208.

versal). On the other hand, alignment is described by a tensor which is even under both P and T. If an isolated system is initially aligned with no net orientation, the system cannot evolve to an oriented state unless we have a T-violating interaction. Alternatively, the presence of an external magnetic field (or some other T-odd axial vector interaction) is a necessary—but not sufficient—condition for an initially aligned state to evolve into one with orientation if there are no significant internal T-violating interactions.

C. Mechanisms for alignment-to-orientation conversion

Several mechanisms for converting alignment to orientation for atomic systems have been proposed and demonstrated. Most of these mechanisms involve an external magnetic field to provide the required preferred direction to allow for a net orientation. The external magnetic field alone cannot produce orientation from alignment. An initially aligned system, in the absence of other interactions, will simply precess about the magnetic field direction via the well-known Hanle effect [9,10]; no net orientation will occur. The equally populated $\pm m$ states precess in such a way as to cause the overall alignment of the system to precess. However, if the electron is subject to a spin-orbit interaction or to hyperfine interaction with the nucleus, the precession of the electron's orbital angular momentum due to the combination of the Zeeman interaction with the external magnetic field and the interaction with the internal fields can lead to a substantial (30% or more) orientation of the atomic state [11–13].

Directional collision processes can also produce oriented atomic states that can be investigated using suitable selective detection. For example, atomic collisions, studied with angle-resolved coincident detection of one of the scattering products and the photon emitted from the other product, select states with an orientation of the excited product [14]. However, this method does not produce a *net* orientation of the atomic sample.

Collisional processes in the presence of an applied magnetic field may produce alignment-to-orientation conversion. Recently, this process has been investigated using velocity-selective excitation with a narrow band laser [15]. The method has been found to produce orientations of a few percent.

In recent years a technique involving orthogonal time-dependent electric and magnetic fields has been used to produce "circular states" (that is, states with complete orientation) in Rydberg atoms [16,17]. This method relies on the mixing of states by the linear Stark effect and is physically distinct from the method introduced in this paper.

Here we describe how interactions with orthogonal static electric and magnetic fields can produce a net atomic orientation from an initially aligned state. In physical terms, it is the combined precessions due to the magnetic interaction and an anisotropic induced electric dipole that allows a net orientation to develop. As we shall see, under appropriate conditions, this arrangement can lead to large atomic orientations.

In the following sections we first describe two experiments: one in the $5d6p\ ^1P$ state of atomic barium, the other in the $F=4$ hyperfine level of the electronic ground state of atomic cesium. Together, these experiments display this new AOC effect over a range of six orders of magnitude in magnetic field values. We then discuss the theory of the effect in the simple case of a ^1S to ^1P atomic dipole transition and its extension to include states with hyperfine structure. We also give a qualitative discussion of the effects of collisions on the observed orientation. From the experimental data and theory, we extract the tensor polarizability of the $5d6p\ ^1P$ state in barium. We conclude with some general remarks about the extension of this technique to other systems.

II. EXPERIMENTS

We have carried out two experiments that demonstrate AOC in atoms subject to orthogonal static electric and magnetic fields. In both cases, the apparatus has been described in detail elsewhere [18,19]; we give just a brief description here.

A. Atomic barium

In the atomic barium experiment, barium vapor is produced in an evacuated stainless steel cross oven illustrated in Fig. 1. The arms of the cross have a diameter of about 3.5 cm. Externally mounted heaters bring the temperature in the central part of the oven to abut 840 K to produce sufficient vapor density (about 10^{12} atoms cm^{-3}) for the experiment [20]. Helium buffer gas, at approximately 0.05 Torr, prevents migration of the barium vapor to the cooled windows at the end of each arm.

The ground-state barium atoms are excited to the $5d6p\ ^1P$ state by 3-nsec pulses of 350-nm radiation produced by frequency doubling the output of a tunable dye

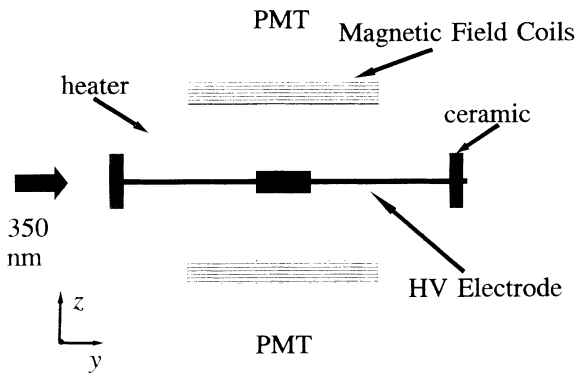

FIG. 1. A schematic diagram of the atomic barium experiment. The static magnetic field is in the z direction. The static electric field is in the x direction. The laser beam propagates along y with its electric field linearly polarized along x. The laser beam and the resulting atomic fluorescence pass between the two electrodes, only one of which is seen in this top view. Two photomultiplier tubes (PMT) view the fluorescence through quarter-wave plates, linear polarizers, and 350-nm bandpass filters.

laser. The dye laser (Continuum TDL-60) is pumped at a repetition rate of 20 Hz by the 532-nm output of a frequency-doubled Continuum 660B YAG (yttrium aluminum garnet) laser. The laser linewidth is about 1.8 GHz (full width at half maximum), which is about the same as the Doppler width of the atomic absorption line. This linewidth is large compared to both the excited state hyperfine splittings and the isotopic shifts of the absorption line [21]. The polarization of the 350-nm radiation is rotated by a half-wave plate to be vertical (i.e., along the x axis), and parallel to the static electric field inside the oven. Brewster angle windows and a series of baffles reduce the stray scattered laser light to negligible levels.

A static magnetic field is produced along the z axis by rectangular field coils. Another pair of coils cancels the vertical component of the Earth's magnetic field. Since the z axis is chosen to be along the local magnetic north-south direction, we can compensate for the horizontal component of the Earth's field by offsetting the current in the z-axis coils.

The static electric field along the x axis is produced by applying a high voltage between two flat, stainless steel electrodes mounted inside the oven. The voltage is turned on approximately 1 μsec prior to the laser pulse and is turned off approximately 1 μsec after the pulse to minimize the potential for electrical discharge through the barium vapor.

The 350-nm fluorescence emitted from the $5d6p\ ^1P$ state along the z direction is monitored by two identical photodetector systems consisting of quarter-wave plates, linear polarizers, 350-nm bandpass filters, and photomultiplier tubes. The output current of the photomultiplier tubes is detected by a pair of Standard Research Systems Model 250 gated integrators, the signals from which are sent to a computer for data analysis. The signals are integrated over the complete fluorescence emission following each laser pulse. The photomultiplier tubes are magnetically shielded, and we verified through independent measurements that the magnetic field has a negligible effect on their gain.

Since we are interested in the net orientation of the atomic excited state, the polarizer combinations are set to monitor the difference between left- and right-circularly polarized light intensity (I_{LCP} and I_{RCP}) emitted along the z axis. The signal we analyze is the circular polarization asymmetry $\mathcal{A}_{\mathrm{CP}}$ defined to be the ratio

$$\mathcal{A}_{\mathrm{CP}}=\frac{I_{\mathrm{LCP}}-I_{\mathrm{RCP}}}{I_{\mathrm{LCP}}+I_{\mathrm{RCP}}} . \tag{3}$$

However, since one detector is monitoring light propagating along the $+z$ direction, while the other monitors light propagating along $-z$, both detectors use identical polarizer settings. We determined the efficiency for circular-polarization analysis by two methods: (a) using one linear polarizer and quarter-wave plate combination as a polarizer and the other as an analyzer, and (b) using one combination with a mirror to retroreflect the light beam through the combination. Both methods yielded an efficiency for discriminating left- from right-circularly polarized light of $(90\pm3)\%$.

The static magnetic field in the z direction is under computer control. The computer steps the magnetic field from about -25 to $+25$ G while averaging the photomultiplier signals from 100 laser pulses for each value of the magnetic field. To focus on the AOC produced by the combination of static electric and magnetic fields, we determine the net $\mathcal{A}_{\mathrm{CP}}$ as the difference between the circular-polarization asymmetry observed with the electric field on and that observed with the electric field off. (We will discuss the static-electric-field-independent effects in Sec. V.) Some care must be exercised to keep the atomic Ba density sufficiently low to avoid the effects of radiation trapping [22] and amplified spontaneous emission [23,24]. Similarly, the helium buffer gas density must be kept below roughly 0.05 Torr to avoid significant collisional depolarization of the excited state.

B. Cs experiment

Most of the apparatus required for the cesium measurements was originally used in an experiment to set an upper limit on the electric dipole moment (edm) of the electron (Ref. [19]). This apparatus has been adapted to provide a careful assessment of atomic cesium alignment-to-orientation conversion, which may cause a so-called E^2B systematic error in the edm experiment. The atomic cesium vapor is contained in two glass cells, approximately $40\times40\times10$ mm^3 in size (Fig. 2). Although two cells are not necessary for the AOC measurement, their presence allowed checks for several possible systematic errors. Heat exchangers attached to the cells raise their temperature to about 50 °C, thereby increasing the vapor density by about a factor of 5 over that at room temperature. A static electric field is produced by applying a high voltage potential difference between the top and bottom surfaces of the vapor cells. These surfaces are coated with aluminum. A voltage of up to 2 kV is supplied to the common center electrode of the cells, while the outer electrodes are at ground potential. This arrangement produces electric fields up to 2 kV/cm in the cells.

Approximately 250 Torr of nitrogen has been added to the cells to increase the relaxation time of the cesium atoms' orientation to about 16 ms while inhibiting elec-

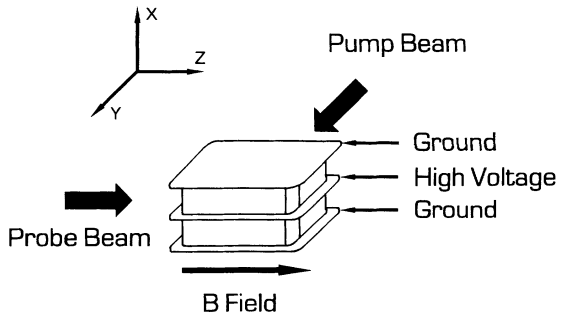

FIG. 2. A schematic of the atomic cesium experimental setup. The circularly polarized pump beams propagates along y. The static electric field is along $\pm x$, and the magnetic field and probe laser beams are along z.

tric discharge.

The cesium cells are kept in a near-zero magnetic field region produced by four layers of high-permeability (μ-metal) shielding and six pairs of coils mounted within the shields. After the shields are degaussed, the residual field within the shields is a few μG and is further reduced in the region of the cells by passing appropriate currents through the coils. The magnetic field is controlled by computer algorithms using the atomic cesium as the probe.

The electronic ground state of cesium is optically pumped by circularly polarized continuous wave radiation tuned to the 894-nm transition connecting the $6S_{1/2}$ $F=3$ hyperfine level of the ground state to the $6P_{1/2}$ excited state. (As usual, F is the quantum number for the total angular momentum of the atom.) Spin exchange and coherence transfer through the excited state result in orientation of the $6S_{1/2}$ $F=4$ hyperfine level along the pump beam direction. (The atomic coherence created here corresponds to an atomic alignment, with no net orientation along the detection direction.) The excited state hyperfine structure is not resolved due to buffer gas collisional broadening. The 894-nm radiation is produced by a Coherent Ti:sapphire ring laser pumped by a Coherent argon-ion laser. The sense of the circular polarization of the pump laser beam is determined by the voltage applied to the crystal of a Pockels cell through which the pump beam passes.

Circularly polarized probe laser beams tuned to the $6S_{1/2}$ $F=4$ to $6P_{1/2}$ transition are directed along the magnetic-field direction, orthogonal to the pump laser beams and to the static electric field, intersecting the pump beams near the center of the cells. The probe laser beams are produced by a Mitsubishi ML2701 semiconductor laser. If the cesium atoms have a net orientation along the probe beam (magnetic field) direction, the absorption coefficient for the probe beam will be different for left-circularly polarized (σ^+) as compared to right-circularly polarized (σ^-) light. The probe beam's circular polarization is modulated between σ^+ and σ^- at 33 kHz using a photoelastic modulator. The differential transmission of the two polarizations results in an intensity modulation proportional to the orientation of the atoms along the probe beam direction. The differential transmission is monitored using photodiodes and lock-in amplifiers.

During data collection, the computer steps the magnetic field through a sequence of field values from 0 to about 60 μG. For each value of the magnetic field, the differential probe signal is averaged for 25 readings from the lock-in amplifiers. This procedure is then repeated with the pump helicity reversed in order to separate the desired AOC signal from any signal associated with the initially prepared orientation. There is a half second wait between the switching of the pump polarization and the data acquisition to allow the atoms to come to equilibrium. To select the signal that is quadratic in the electric field, the above procedure is repeated with the electric field reduced to zero and the difference is taken between the "field on" and "field off" signals. There is a 12-sec wait between switching the electric field and data acquisition to allow charging currents to subside to negligible levels.

III. THEORY

A. $j=0$ to $j=1$ transition

Here we present the theory of AOC in orthogonal static electric and magnetic fields for the case of an atomic electric-dipole transition between a $j=0$ lower state and a $j=1$ excited state with no spin-orbit or hyperfine interactions. Later we discuss the extension of this calculation to include hyperfine structure and the effects of collisions.

We begin with the appropriate perturbation Hamiltonians for static magnetic and electric fields. As usual, the external magnetic-field interactions are given by the Zeeman Hamiltonian

$$\hat{H}_z = g_J \mu_B B_z \hat{J}_z \equiv h\beta \hat{J}_z \ , \tag{4}$$

where h is Planck's constant, μ_B is the Bohr magneton, g_J is the gyromagnetic ratio, and B_z is the static magnetic field assumed to be in the z direction. The last equality defines the parameter β.

For a static electric field E_x in the x direction, the perturbation can be represented (to order E^2) with the effective Hamiltonian [25,26] acting within the single excited state j manifold

$$\hat{H}_E = -\tfrac{1}{2}\alpha_0 E_x^2 \hat{I} - \tfrac{1}{2}\alpha_2 E_x^2 \frac{3\hat{J}_x^2 - \hat{J}^2}{j(2j-1)} \ . \tag{5}$$

α_0 is the scalar polarizability of the state, and α_2 is the tensor polarizability. (We shall henceforth ignore the scalar polarizability term since it results only in a common shift of the excited state m levels.) We are interested in the differential shift caused by the tensor polarizability.

The resulting Hamiltonian matrix for a $j=1$ state takes the form

$$H_{ij}/h = \begin{bmatrix} \beta+p & 3p & 0 \\ 3p & -\beta+p & 0 \\ 0 & 0 & -2p \end{bmatrix} , \tag{6}$$

where we have written the matrix elements in the nonstandard order $m=+1$, -1, and 0 in order to emphasize the block-diagonal structure of the matrix. The symbol p is defined as

$$p = \frac{1}{4}\frac{\alpha_2 E_x^2}{h} \ . \tag{7}$$

Since this matrix is 2×2 block diagonal, the eigenvalues and eigenvectors can be found exactly. The energy eigenvalues are

$$\begin{aligned} E_+/h &= p + \sqrt{9p^2+\beta^2} \ , \\ E_-/h &= p - \sqrt{9p^2+\beta^2} \ , \\ E_0/h &= -2p \ . \end{aligned} \tag{8}$$

The energy eigenvectors can be written as linear combinations of the eigenvectors of $\hat{J}_z$:

$$|E_+\rangle = A|m=+1\rangle - C|m=-1\rangle ,$$
$$|E_-\rangle = C|m=+1\rangle + A|m=-1\rangle , \quad (9)$$
$$|E_0\rangle = |m=0\rangle .$$

The state coefficients A and C are given by

$$A=\left[\frac{\gamma+\beta}{2\gamma}\right]^{1/2},$$
$$C=\left[\frac{\gamma-\beta}{2\gamma}\right]^{1/2}, \quad (10)$$

where $\gamma=\sqrt{9p^2+\beta^2}$.

The state vector for the excited state can be written either as a superposition of energy eigenstates or as a superposition of angular momentum eigenstates:

$$|\Psi(t)\rangle = \sum_k b_k(t)|E_k\rangle = \sum_m c_m(t)|m\rangle , \quad (11)$$

where the summation index k runs over $+$, $-$, and 0, while m is $+1$, -1, and 0. Since the net orientation of the $j=1$ state is proportional to $|c_{+1}(t)|^2-|c_{-1}(t)|^2$, and since the $m=0$ sublevel does not radiate in the z direction, we may safely ignore the $m=0$ state in what follows. As we shall see, it is crucial that the excited state prepared by the laser pulse is not an energy eigenstate in order to observe AOC.

In the following development we let $t=0$ be the instant of excitation of the system. With the laser beam electric field linearly polarized in the x direction, it is easy to show that

$$c_{+1}(t=0) = -c_{-1}(t=0) \equiv M , \quad (12)$$

where M is proportional to the product of the laser electric-field amplitude and the transition dipole moment matrix element. The state coefficients $\langle E_{+,-}|m\rangle$ from Eq. (9) yield the energy eigenstate coefficients

$$b_+(t=0) = +M(A+C) ,$$
$$b_-(t=0) = -M(A-C) . \quad (13)$$

To find the $c_m(t)$ needed to compute the circular-polarization asymmetry, we use

$$b_{+,-}(t) = b_{+,-}(0)e^{-(i/\hbar)E_{+,-}t} . \quad (14)$$

Straightforward algebra then gives

$$|c_{\pm 1}|^2 = \frac{e^{-\Gamma t}}{2}[1 \pm 2AC(A^2-C^2)(1-\cos\Delta\omega t)] , \quad (15)$$

where $\hbar\Delta\omega = E_+ - E_-$. We have added a phenomenological exponential damping factor to account for the radiative decay to the excited state. Γ is the reciprocal of the excited state lifetime (approximately 12 nsec for barium) [27]. The state coefficients have been normalized so that $|c_{+1}(t=0)|^2+|c_{-1}(t=0)|^2=1$.

From Eq. (15) we find the circular-polarization asymmetry (which for the $j=1$ case is just twice the orientation):

$$\mathfrak{A}(t) = |c_{+1}|^2 - |c_{-1}|^2$$
$$= 2AC(A^2-C^2)(1-\cos\Delta\omega t)e^{-\Gamma t} . \quad (16)$$

In our experiment, we integrate the resulting signal over time. After a bit of algebra we find that the time-integrated circular-polarization asymmetry $\mathcal{A}_{CP}$ is given by

$$\mathcal{A}_{CP} = \frac{3p\beta}{9p^2+\beta^2+\frac{\Gamma^2}{16\pi^2}} . \quad (17)$$

Note that the sign of the circular-polarization asymmetry depends both on the sign of the magnetic field (via β) and on the sign of the tensor polarizability (via p). For small values of the electric and magnetic fields (so that $9p^2+\beta^2 \ll \Gamma^2/16\pi^2$), $\mathcal{A}_{CP}$ is proportional to E^2B. This low-field-dependent signal was noted and discussed as a possible source of systematic error in Ref. [19].

As an aside, we point out that the result stated in Eq. (17) could be calculated directly using the Breit equation [10,28–30]. For example, the time-integrated intensity of right-circularly polarized light is given by

$$I_{RCP} = \sum_{j,k} \frac{F_{jk}G_{kj}}{\Gamma - i\omega_{kj}} \quad (18)$$

with the appropriate excitation (F_{jk}) and detection (G_{kj}) matrices. However, the crucial physics of the state mixing induced by the orthogonal electric and magnetic fields is not so transparent in that derivation.

B. Hyperfine structure effects

Both ^{135}Ba (6.6% natural abundance) and ^{137}Ba (11.3% natural abundance) have nuclear spin $I=\frac{3}{2}$ and possess hyperfine structure. Since the hyperfine structure of the $(5d6p)\,^1P$ state is known (Ref. [21]), it is straightforward, but tedious, to evaluate the required matrix elements of the static electric- and magnetic-field perturbations and the consequent state mixings. These results are used to compute the excitation and detection matrices in the Breit equation, Eq. (18), and finally to determine $\mathcal{A}_{CP}$ due to ^{135}Ba and ^{137}Ba. The hyperfine structure itself will lead to AOC in the presence of an external magnetic field (Refs. [7] and [11–13]). Thus we compute $\mathcal{A}_{CP}$ both with and without a static electric field.

We then subtract the zero static-electric-field part from the total $\mathcal{A}_{CP}$ to compare with the results of our experiment. For the conditions of our experiment, the electric-field-dependent $\mathcal{A}_{CP}$ associated with the odd isotopes (weighted by their natural abundance) is only a few percent, but has a magnetic-field dependence somewhat different from that of the even isotopes, which have no hyperfine structure. The difference is due to the incipient hyperfine uncoupling of the states as the magnetic field increases.

IV. CLASSICAL MODEL

Although the quantum mechanical calculation presented in Sec. III is straightforward, we believe that it is

helpful to have a more intuitive picture of how a net orientation arises from an initially aligned system. The crucial physical ingredients in this picture are the precession of the electron's orbital angular momentum due to the interaction of the atom's magnetic moment with the external magnetic field combined with a precession caused by the induced electric dipole moment (proportional to the tensor polarizability).

Let us begin with the tensor polarizability effect. We model the atom as an anisotropic polarizable object with different polarizabilities along and orthogonal to the orbital angular momentum. If the electric field and the angular momentum vectors are neither aligned nor orthogonal, then the induced dipole moment $\vec{p}=\vec{\vec{\alpha}}\vec{E}$ (where $\vec{\vec{\alpha}}$ is the polarizability tensor) will not be parallel to $\vec{E}$. Hence, the induced electric dipole will experience a torque $\vec{p}\times\vec{E}$.

For the magnetic interaction, we take the atom's magnetic moment $\vec{\mu}$ to be antiparallel to the orbital angular momentum. Thus, the orbital angular momentum will experience a torque $\vec{\mu}\times\vec{B}$.

The quantum state produced in the barium experiment by the pulsed laser under the conditions described in Sec. III gives a zero expectation value for each of the Cartesian components of the angular momentum vector. In addition, the state has $\langle\hat{J}_y^2\rangle=\langle\hat{J}_z^2\rangle=\hbar^2$ and $\langle\hat{J}_x^2\rangle=0$. Thus the appropriate classical analog of this state is an ensemble of angular momentum vectors distributed uniformly in direction in the yz plane.

Since the angular momentum vectors are initially orthogonal to the electric field, there is at first no torque due to the induced electric dipole. However, as the magnetic torque causes the angular momentum vectors to precess out of the yz plane, the induced electric dipole is no longer parallel to the electric field and a $\vec{p}\times\vec{E}$ torque results. This torque causes the angular momentum vectors to precess about the x axis. Each angular momentum vector in the ensemble and its partner, pointing in the opposite direction, experience an electric torque of the same sign, and tend to become oriented in the same direction along the z axis. The sense of that rotation depends on both the sign of the tensor polarizability and on the sense of the magnetic field, which determines the original rotation out of the yz plane. An analogous argument for the atomic cesium case, in which the atoms are initially oriented along y, is straightforward. The details of this classical model will be presented in a subsequent paper [31].

V. EXPERIMENTAL RESULTS

A. Barium

Figure 3 shows the results of measuring the circular polarization asymmetry as a function of magnetic field for the atomic barium $5d6p\ ^1P$ state with two different values of the static electric field. In comparing the results of the measurements with the prediction of Eqs. (17) (for the even isotopes) and (18) (for the odd isotopes), we must take into account two effects. First, we multiply the calculated $\mathcal{A}_{\rm CP}$ by 0.90 in order to correct for the efficiency of our circular polarization analyzers.

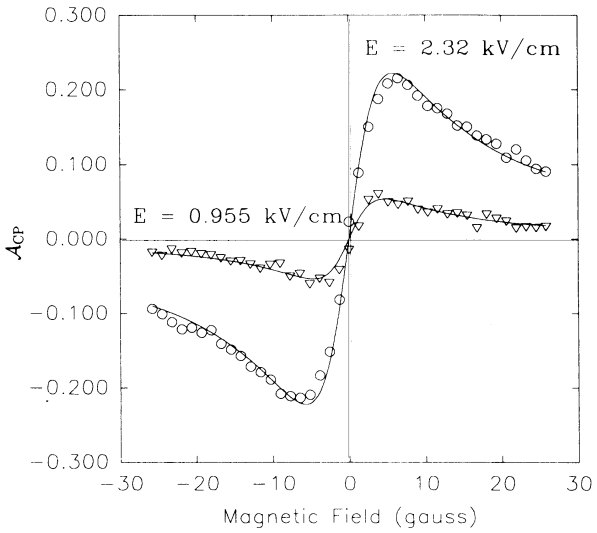

FIG. 3. The circular-polarization asymmetry $\mathcal{A}_{\rm CP}$ for the atomic barium $5d6p\ ^1P$ state plotted as a function of magnetic field for two different values of the static electric field. The circles (triangles) represent the experimental data with an electric field of 2.32 kV/cm (0.955 kV/cm). As expected, $\mathcal{A}_{\rm CP}$ has a smaller peak value for the smaller electric field and peaks at a smaller value of B. The solid curves are the results of a least-squares fit of the theoretical calculation. The tensor polarizability is the only adjustable parameter.

Second, collisions between the excited barium atoms and the helium buffer gas can lead to a depolarization of the excited state. Calculations using the density matrix formalism [32] indicate that collisions lower the overall observed asymmetry (as expected) and change slightly the observed signal shape (as a function of magnetic field). Using the standard Hanle effect (linearly polarized detection in a static magnetic field alone), we determined that the depolarization rate (strictly speaking the alignment-relaxation rate) is approximately 25 MHz/Torr for the conditions of our experiment. In practice, we kept the buffer gas pressure below 0.05 Torr when taking data. By extrapolating runs carried out at higher helium pressures, we are confident that collisional depolarization should be insignificant at these lower pressures, but to be conservative we have included a 2% experimental uncertainty to account for possible residual collisional depolarization.

The results of fitting our theoretical calculations to the data are shown in Fig. 3 as solid curves. The only adjustable parameter is the tensor polarizability α_2. The fit is excellent and yields a value for the tensor polarizability of the $5d6p\ ^1P$ state:

$$\alpha_2=+1.31\pm0.15\ \text{MHz}/(\text{kV/cm})^2\ , \tag{19}$$

where we have combined in quadrature the uncertainties in the tensor polarizability due to the fit (±0.5%), the calibration of the polarizer efficiency (±3%), the residual collisional depolarization (±2%), the electrode spacing (±10%), and the applied voltage (±2%) to find the overall experimental uncertainty.

The tensor polarizability for the $5d6p\ ^1P$ state of ^{138}Ba

was measured previously [33] to be +1.37 MHz/(kV/cm)^2 with an uncertainty of about 2% by an atomic beam, cw laser experiment. Our result, though less precise, is in good agreement with this value. The precision of our results is limited by the relatively crude electrodes (originally designed for another experiment) that we used.

B. Electric-field-independent AOC

As mentioned above, the Ba atoms with hyperfine structure are expected to show a circular polarization asymmetry even in the absence of a static electric field. However, for the range of magnetic-field values used in our experiment, the net effect of the hyperfine-induced AOC is less than 1%. [Our calculations show that the three different excited state hyperfine levels give individual AOC effects with phase differences that tend to reduce the overall effect. An analogous cancellation was observed in AOC experiments in atomic sodium (Ref. [13]).] Nevertheless, we have observed an electric-field-independent $\mathcal{A}_{CP}$ that is strongly dependent on the intensity the exciting laser beam. We attribute this effect to AOC by the combined action of the static magnetic field and the electric field of the laser beam. (Our AOC effect is proportional to E^2. It is well known [34] that a time-dependent field can polarize an atom with a resulting tensor polarizability much like the static field case.) We plan to explore this effect in subsequent experiments.

C. Results in Cs

The cesium results are summarized in Fig. 4. The difference between the electric "field on" and "field off" signals is plotted as a function of the applied magnetic field. As discussed previously, this signal is proportional to the orientation of the cesium vapor along the magnetic-field direction. The solid line shows the results of fitting the simple theoretical model Eq. (17) to the data, using a previous measurement of the tensor polarizability of the Cs ground state [35]. A numerical calculation [36] of the evolution of the state amplitudes for all nine magnetic sublevels of the $F=4$ state confirms that Eq. (17) should correctly describe the shape of the alignment-to-orientation conversion data, provided that a *single* spin relaxation rate is adequate to describe the system. The model, while matching the gross features of the data and correctly predicting the quadratic field dependence, is obviously inadequate for describing the precise shape of the cesium data. The discrepancy is due to the more complex structure of the cesium $F=4$ level and the high buffer gas pressure, which results in substantial collisional depolarization rates which differ for the different atomic coherences. Unfortunately, to account for collisions in the $F=4$ case quantitatively, a full density matrix calculation would have to be undertaken with a knowledge of all of the relaxation rates of all orders of the possible multipoles of the $F=4$ state. A density matrix calculation [32] for the $j=0$ to 1 case suggests that the inclusion of relaxation due to collisions can (for reasonable values of the relaxation rates for the alignment and orientation), result in modifications of the line shape similar to those observed in the cesium data. Though the tensor polarizability of the cesium ground state is known (Ref. [35]), a quantitative comparison with our data is not possible due to the lack of a complete model and insufficient information about the relaxation rates of the higher-order multipoles of the cesium density matrix.

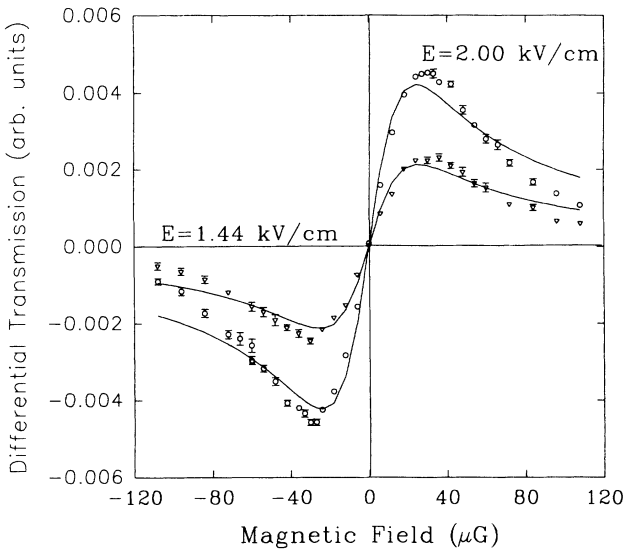

FIG. 4. Atomic cesium experimental results. The probe beam differential transmission (proportional to the net orientation of the atoms along the magnetic field) is plotted as a function of the magnetic field. The triangles (circles) represent the experimental results taken with an electric-field strength of 1.44 kV/cm (2.0 kV/cm). The solid curves are the result of fitting Eq. (17) to the data with a single spin relaxation rate and an overall amplitude as the adjustable parameters.

VI. CONCLUDING REMARKS

We have shown that orthogonal electric and magnetic fields can produce substantial alignment-to-orientation conversion in atomic systems. These effects have been observed in an excited state of barium and in the ground state of cesium. The results span six orders of magnitude in relaxation time and magnetic field. The large asymmetries observed in atomic barium with rather modest applied electric fields indicate that, with an improved electrode structure, the method introduced here could be used for precise measurements of atomic tensor polarizabilities. These polarizabilities are useful tests of calculations of atomic radial matrix elements.

In addition, this effect needs to be taken into account as a possible source of systematic errors in experiments that use atomic or molecular orientation as a test for parity-violating or time-reversal-invariance-violating interactions.

ACKNOWLEDGMENTS

We would like to thank Daniel Krause, Jr. for technical assistance. This work was supported by the National Science Foundation (RUE, RUI, and ILI programs) and by Amherst College. K.J.'s efforts were supported in part by a research stipend from the APS Laser Science Topical Group.

[1] L. R. Hunter, Science **252**, 73 (1991).
[2] E. D. Commins, Phys. Scr. T **46**, 96 (1993).
[3] E. D. Commins, Am. J. Phys. **61**, 778 (1993).
[4] U. Fano and J. H. Macek, Rev. Mod. Phys. **45**, 553 (1973).
[5] A. C. Kunmel, G. O. Sitz, and R. N. Zare, J. Chem. Phys. **88**, 7357 (1988).
[6] See, for example, K. Blum, *Density Matrix Theory and Applications* (Plenum, New York, 1981); N. Andersen, J. W. Gallagher, and I. V. Hertel, Phys. Rep. **165**, 1 (1988).
[7] J. C. Kemp, J. H. Macek, and F. W. Nehring, Astrophys. J. **278**, 863 (1984).
[8] For a general discussion of such processes and other topics relevant to the present development, see E. B. Alexandrov, M. P. Chaika, and G. I. Khvostenko, *Interference of Atomic States* (Springer-Verlag, New York, 1993).
[9] W. Hanle, Z. Phys. **30**, 93 (1924).
[10] *The Hanle Effect and Level-Crossing Spectroscopy,* edited by G. Moruzzi and F. Strumia (Plenum, New York, 1991).
[11] M. Krainska-Miszczak, J. Phys. B **12**, L205 (1979).
[12] M. Krainska-Miszczak, J. Phys. B **12**, 555 (1979).
[13] X. L. Han and G. W. Schinn, Phys. Rev. A **43**, 266 (1991).
[14] B. W. Moudry, O. Yenen, and D. H. Jaecks, Phys. Rev. Lett. **71**, 991 (1993).
[15] A. G. Petrashan, V. N. Rebane, and T. K. Rebane, Opt. Spectrosc. **70**, 424 (1991).
[16] D. Delande and J. C. Gay, Europhys. Lett. **5**, 303 (1988).
[17] J. Hare, M. Gross, and P. Gay, Phys. Rev. Lett. **61**, 1938 (1988).
[18] S. Wielandy, T.-H. Sun, R. C. Hilborn, and L. R. Hunter, Phys. Rev. A **46**, 7103 (1992).
[19] S. A. Murthy, D. Krause, L. Li, and L. R. Hunter, Phys. Rev. Lett. **63**, 965 (1989).
[20] E. Hinnov and W. Ohlendorf, J. Chem. Phys. **50**, 3005 (1969).
[21] P. Grundevik, H. Lundberg, L. Nilsson, and G. Olsson, Z. Phys. A **306**, 195 (1982).
[22] T. Holstein, Phys. Rev. **83**, 1159 (1951).
[23] M. Taleb, G. Fabre, and R. Stringat, J. Phys. Colloq. (France) **47**, C-577 (1987).
[24] A. Kallenbach and M. Koch, J. Phys. B **22**, 1691 (1989); **22**, 1705 (1989).
[25] A. Khadjavi, A. Lurio, and W. Happer, Phys. Rev. **167**, 128 (1968).
[26] J. R. P. Angel and P. G. H. Sandars, Proc. Roy. Soc. A **305**, 125 (1968).
[27] L. O. Dickie and F. M. Kelley, Can. J. Phys. **49**, 2630 (1971).
[28] G. Breit, Rev. Mod. Phys. **5**, 91 (1933).
[29] P. A. Franken, Phys. Rev. **121**, 508 (1961).
[30] A. Corney, *Atomic and Laser Spectroscopy* (Oxford University Press, Oxford, 1978).
[31] R. C. Hilborn (unpublished).
[32] M. Kozlov (private communication).
[33] K. A. H. van Leeuwen and W. Hogervorst, Z. Phys. A **310**, 37 (1983).
[34] A. M. Bonch-Bruevich and V. A. Khodovoi, Usp. Fiz. Nauk. **93**, 71 (1967) [Sov. Phys. Usp. **10**, 637 (1967)].
[35] H. Gould, E. Lipworth, and M. C. Weisskopf, Phys. Rev. **188**, 24 (1969).
[36] L. R. Hunter (unpublished).